

Experimental research and finite element analysis on seismic behavior of CFRP-strengthened seismic-damaged composite steel-concrete frame columns



Sheng Peng^a, Chengxiang Xu^{a,*}, Mengxiao Lu^b, Jianming Yang^a

^a Department of Civil Engineering, School of Urban Construction, Wuhan University of Science and Technology, Wuhan 430065, PR China

^b School of Urban Construction, Yangtze University, Jingzhou 434023, PR China

ARTICLE INFO

Keywords:

Carbon fiber reinforced polymer strengthening
Composite steel-concrete frame columns
Seismic damage
Finite element analysis
Seismic behavior

ABSTRACT

Four composite steel-concrete frame columns were constructed to investigate the seismic performance of seismic-damaged composite steel-concrete frame columns strengthened with carbon fiber reinforced polymer. The test consisted of pre-damage loading, rehabilitation with carbon fiber reinforced polymer and destruction tests under lateral cyclic loading. The effectiveness of strengthening seismic-damaged columns with carbon fiber reinforced polymer and the strengthening effect on different degrees of seismic damage were studied. Also, based on the test data, various parameters were obtained, including the hysteretic loops, skeleton curves, axial compression ratio, number of pasted layers of carbon fiber reinforced polymer, ductility, dissipative ability, ultimate strength, stiffness degradation, etc. The results revealed that the failure mode of all the columns was bending failure. The study indicates that the rehabilitated columns can reach or even exceed the level of their original seismic performance before seismic damage up to a certain extent of damage level. Composite steel-concrete frame columns strengthened with carbon fiber reinforced polymer sheets were simulated using the finite element analysis software ABAQUS. The comparison of the results of the conducted analytical study with the experimental results revealed that they are basically consistent with each other.

1. Introduction

The frame column structure composed of sections of steel-reinforced concrete has been widely used in super-high building structures and large span structures due to its high load-carrying capacity, good seismic performance, and other advantages [1]. Seismic evaluation and strengthening of composite steel-concrete structures are not mentioned in guidelines publications, such as “Standard for Seismic Appraisal of Buildings” (GB50023-2009), “Technical specification for seismic strengthening of buildings” (JGJ116-2009) and “Technical guidelines for seismic evaluation and strengthening of post-earthquake buildings”. In practical engineering, the carbon fiber sheet has received considerable attention due to its high-strength, light-weight, high corrosion resistance, and ease of fabrication, etc. This effective strengthening method using composite steel-concrete structures has become more and more widely used in the United States, Canada, Japan, and recently, Europe. In China, the research and application of carbon fiber reinforced polymer (CFRP) for strengthening reinforced concrete structures began in 1997.

Several studies have been conducted on the seismic performance

and behavior under reinforced concrete [2–4] and composite steel-concrete columns [5–7], steel fiber reinforced concrete (SFRC) [8] and concrete-encased composite structures of concrete frame and steel-concrete composite columns, as well as the behavior under ultra-high performance fiber reinforced concrete (UHPFRC) [9–11] and numerical simulation methods [12,13]. The design calculation theory and construction method are given in the building codes, such as ACI 318-05code [14], JGJ 138-2001 specifications [15], ALJ-SRC standard [16] and the AISC Manual of Steel Construction [17].

In experimental research, these include, a study on seismic-damaged RC column, frame and beam-column joints strengthened with stainless steel wire mesh composite [18], CFRP [19], and epoxy resin injection [23–25], respectively. The method of CFRP-strengthened seismic-damaged exterior joints in composite frame consisting of CFSST columns and steel beams were proposed by Xu et al. [20]. A detailed investigation on the assessment of the performance of new material was presented by Zhang [21], and the theoretical development of the mechanical properties of new material with the time was extensively studied by Wang [22]. According to published experimental studies, RC structures could be strengthened with new material [21,22]. Idris and

* Corresponding author.

E-mail address: cx_xu@sina.com (C. Xu).

Ozbakkaloglu studied the seismic behavior of the seismic-damaged high-strength concrete-filled tube columns strengthened with FRP subjected to constant axial load and cyclic lateral loads [26–28], and summarized the Confinement model of FRP-confined high-strength concrete [32,33]. However, very few methods and experimental studies are available on seismic-damaged composite steel-concrete frame column structure. There are rarely reports on seismic performance and failure mechanism of seismic-damaged composite steel-concrete frame column structures reinforced with strengthening materials. Here, seismic-damaged composite steel-concrete column structure strengthened with CFRP are put forward.

In this study, cyclic loading tests were performed on four composite steel-concrete columns to investigate the effect of the strengthening of seismic-damaged composite steel-concrete with CFRP on the performance of frame columns. The tests included horizontal load testing, horizontal displacement testing and recording of the load-displacement hysteresis loops of the specimens. The mechanical process, failure mode, hysteretic characteristics, skeleton curves, ductility and energy dissipation capacity were taken into account. The simulation calculation was carried out using the ABAQUS software.

Simulation calculation and experimental results are compared to verify the rationality and the experimental results. The authors hope to provide references for seismic-damaged composite steel-concrete frame column structure strengthened with CFRP.

2. Experimental program

2.1. Test specimens

Four composite steel-concrete frame columns, with different degrees of post-earthquake seismic damage, were designed for the tests, and numbered from SRC-1 to SRC-4.

The data shown in Table 1 indicate that specimens SRC-1, SRC-2, SRC-3, SRC-4 are under the same axial compression ratio, and have the same shear span ratio and concrete strength grade. Accordingly, they can be considered to have the same degree of damage and strengthening level. Based on the same considerations, specimens SRC-2, SRC-3 and SRC-4 are also considered to have the same number of strengthening CFRP layers [23]. Besides, the composite steel-concrete frame columns are short columns.

Although specimen SRC-1 has not been strengthened and SRC-2 has been strengthened, both SRC-1 and SRC-2 specimens are undamaged. A displacement angle of 1/100 was used to simulate the moderate damage of specimen SRC-3, while a displacement angle of 1/50 was used to simulate the severe damage of specimen SRC-4. The test specimens had a rectangle cross section of 200 mm × 270 mm and the cover thickness of the concrete specimens was kept at 25 mm. The cross-section reinforcement ratio of the specimens is 1.6% and the stirrup ratio is 0.68%, while the steel ratio of the specimens is 4.84%. To ensure the same quality of concrete the C40 commercial concrete was used, pouring from the same batch, with 28 days of maintenance.

The properties of the materials were controlled by the material categories and material specifications given in Table 2. The configurations of a specimen cross-section and the diagram of strengthening by CFRP are shown in Fig. 1. Specifically, the arrangement of the strain gauges on the specimens is shown in Fig. 1a. The strains of the

longitudinal (S1 ~ S3) section of steel were measured by the strain gauges. The composite steel-concrete column base was strengthened with CFRP. The CFRP was pasted in the direction perpendicular to the axis of the column using the circular uniform packing method. The layer number is two and the lap length is 150 mm. while the strengthening height is 500 mm.

2.2. Materials properties

The properties of the materials, such as concrete, steel, bar CFRP and mucilage are listed in Table 2.

2.3. Test device and loading system

The columns were constructed and tested at the Civil Engineering Experiment Center of Yangtze University. All specimens were tested after 28 days of maintenance.

Premixed concrete was used. To determine the average concrete compressive strength, three cylinders were tested for each specimen. The measured compressive strength of concrete was 39.6 MPa. The test, performed under lateral cyclic loading, consisted of pre-damage loading, rehabilitation with CFRP and destruction tests.

The test set-up and loading system are shown in Fig. 2(b). The lateral load was applied by a servo-controlled hydraulic actuator at the upper column end, using a displacement-controlled tester at a speed of 10 mm/min. A hinge support was used at the bottom of each column of the axial load reaction frame, allowing the reaction frame to rotate [5]. The specimens can be rigidly anchored to the ground through the ground beam which was placed at the bottom of the specimens. The upper end loading scheme was adopted to simulate the $P - \Delta$ effect caused by the applied axial compressive load acting on the lateral displacement of the columns. The axial compressive load was applied by a hydraulic jack installed at the upper end of column and it remained constant. The tests of the loading system followed the JGJ101-96 guidelines [29].

The columns were laterally subjected to a predetermined cyclic displacement history as indicated in Fig. 2(a), which shows that the peak displacements were increased in multiples of the yielding displacement. The load control occurred before the specimens yielded, and the displacement control occurred after the specimens yielded.

The specimens were subjected to one cycle before yielding and three successive cycles after yielding. The experiment was stopped when the load dropped below 85% of the ultimate load, or the specimens were unable to bear the axial force.

2.4. Reinforcement of specimens

The reinforcement of the specimens was performed following the GB/CECS146-2003 guidelines. To prevent the transfer of plastic hinge during the tests, the reinforcement height should be higher than the plastic hinge, at the bottom of the columns.

Before the reinforcement, the surface of the concrete should be ground until its aggregate was exposed [29] and the fillet radius processed to 20 mm at the bottom as indicated in Fig. 1(b).

Table 1
Parameters of specimens.

Specimen	Damage degree	Axial compression ratio	Shear span ratio	Concrete strength grade	CFRP layer number	Strengthened level
SRC-1	Undamaged	0.32	1.5	C40	–	No
SRC-2	Undamaged	0.32	1.5	C40	2	yes
SRC-3	Moderate damaged	0.32	1.5	C40	2	yes
SRC-4	Severe damaged	0.32	1.5	C40	2	yes

Table 2
Materials properties.

Material	Specification	Elastic modulus E_s /MPa	Tensile strength f_y /MPa	Compressive strength f_u /MPa	Yield strength f_y /MPa	Ultimate strength f_u /MPa
Concrete	150 mm length cube	–	–	39.6	–	–
II16 steel	Q235B	2.01×10^5	–	–	264.5	405.8
Longitudinal bar	HRB400	2.05×10^5	–	–	375.7	515.6
Stirrup	HPB300	2.10×10^5	–	–	312.4	443.1
CFRP	CJ300-I	2.50×10^5	3560	–	–	–
Mucilage	CFRP mucilage	2476	42	–	–	–
	Crack repair mucilage	1563	30	–	–	–

3. Experimental results and analysis

3.1. Experimental phenomena and failure mode

The test consisted of two parts: pre-yielding and post-yielding.

Before yielding, the specimens were in the elastic stage, and the value of the residual deformation was small. The deformation recovered when the specimen was unloaded. When the horizontal displacement increased to about 3.6 mm, the first crack appeared on the tensile side at the column bottom end. When the horizontal displacement increased to ± 9 mm, the longitudinal reinforcement and steel flange yielded on the tensile side, and oblique cracks developed at the column bottom end.

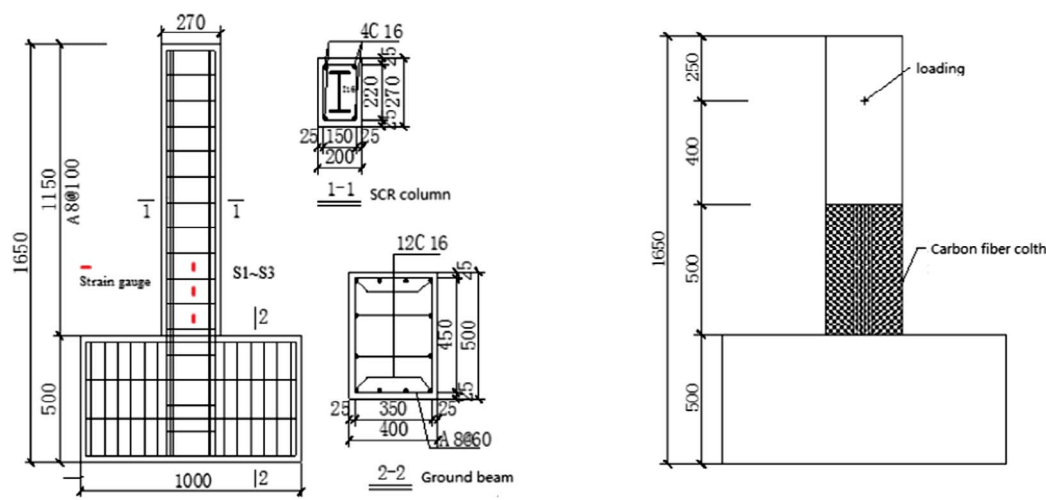
After yielding, the horizontal displacement increased to ± 18 mm, existing cracks continued to develop and new cracks appeared at the column bottom end. With the increase of the number of cracks and their width, the specimens of bearing capacity significantly degraded and some apparent X-shaped cross inclined cracks were observed. When the horizontal displacement increased to ± 27 mm, the concrete-flake-off extended at the column bottom zone. With the circle of reverse unloading-loading, the concrete-flake-off position moved towards the middle of the column. When the horizontal displacement increased to ± 36 mm, the cracks transfix and the concrete-flake-off appeared, and the stirrups and longitudinal reinforcements were exposed and bent. When the horizontal displacement increased to about ± 45 mm, the stirrups and part of longitudinal reinforcements were damaged. The bearing capacity of the specimens dropped below 85% and the testing stopped.

At the end of the test, the lateral load dropped rapidly and the

specimens lost the bearing capacity. However, the core concrete had little damage due to the restraint of the structural steel located in the center zone of the cross section. Flexural failure of the specimens occurred in the plastic hinge zone. The failure mode of specimen SRC-1 is shown in Fig. 3(a) and the failure mode of the limit state at the bottom end of the columns of the different seismic-damaged CFRP-strengthened specimens, including SRC-2, SRC-3 and SRC-4, are presented in Fig. 3(b)–(d). When the horizontal displacement is shorter than ± 18 mm, the CFRP did not experience obvious change, and sporadic brittle crack occurred at weak positions in the CFRP viscose. When the horizontal displacement increased to 18 mm, folding appeared on the CFRP. Specifically, there were no cracks in the SRC-2 specimen, small horizontal cracks occurred in the SRC-3 specimen on the tensile side at the bottom end of the column and horizontal cracks occurred in the SRC-4 specimen on the tensile side at the bottom end of the column with clear crack voice at the weak positions in the CFRP viscose.

When the horizontal displacement increased to ± 27 mm, horizontal cracks began to appear in the CFRP at the bottom end of the column of specimen SRC-2, and existing cracks continued to develop at bottom end of the column of specimen SRC-3 and specimen SRC-4 had new horizontal cracks in the CFRP on its tensile side. Horizontal cracks continued to spread and close due to the cyclic loading and the crack width progressively grew.

When the horizontal displacement increased to ± 36 mm, the existing cracks continued to develop in the CFRP at the bottom end of the column, and the number of new cracks and their width continuously increased and formed the horizontal transfixion fracture. During cyclic loading, large horizontal transfixion fracture appeared at the bottom end of the column when the horizontal displacement increased to about

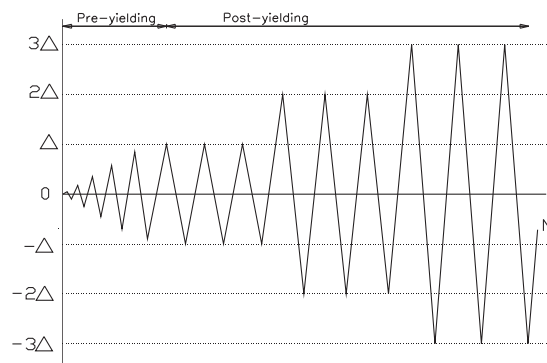


(a) Specimen dimension and steel details

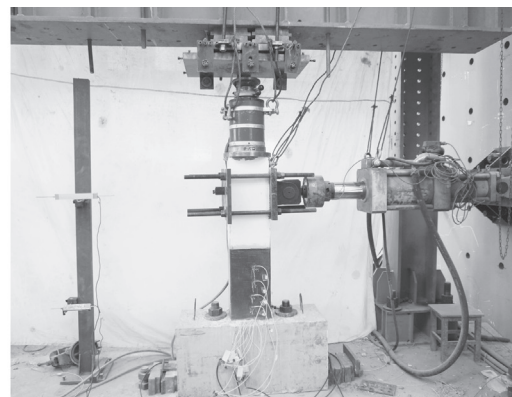
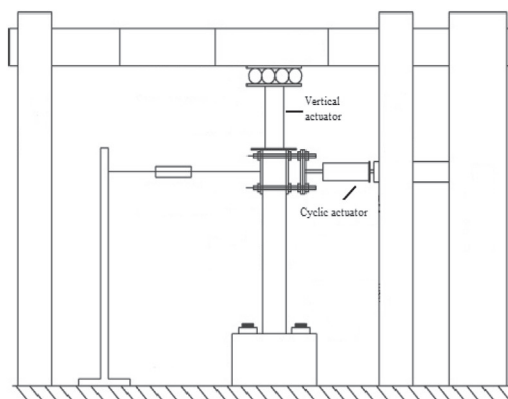
(b) Strengthening of carbon fiber sheets at column bottom

Note: dimensions are in mm

Fig. 1. Specimen dimension and Strengthening.

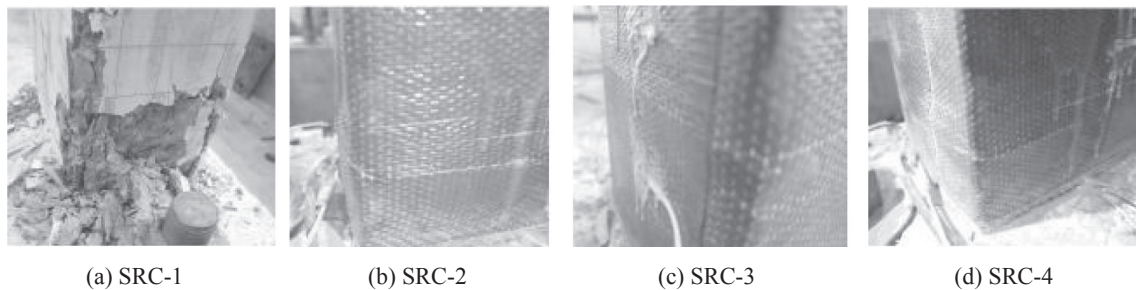


(a) Loading system for horizontal displacement



(b) Test set-up for cyclic loading test

Fig. 2. Test set-up and loading system.



(a) SRC-1

(b) SRC-2

(c) SRC-3

(d) SRC-4

Fig. 3. Failure modes of specimens.

45 mm. Concrete crushing appeared on the compressive side at the column bottom end, and a drum curve appeared in the CFRP on the tension side at the bottom end of the column.

When the horizontal displacement increased to ± 54 mm, the drum curve continued to develop in the CFRP, and horizontal visible cracks appeared at the bottom end of the column of specimen SRC-4. Then, the lateral load dropped rapidly, the specimens lost their bearing capacity, and the testing stopped. However, the core concrete had little damage due to the restraint of the structural steel located in the center zone of the cross section. When the horizontal displacement increased to ± 63 mm during cyclic loading, the horizontal transfixion fracture appeared at the bottom end of the column of specimens SRC-2 and SRC-3.

Then, the bearing capacity of the specimens dropped below 85% and the testing stopped.

3.2. Hysteretic curve

The hysteretic curve is a load-displacement relationship curve of the

specimen under cyclic loading. As shown in Fig. 4, the hysteretic curve is described by the measured lateral load and the displacement at the top end of the column, which is an important representation of seismic performance. The following observations can be made from the results shown in Fig. 4:

When a horizontal load was not bigger than the yield load, the curve slope changed slightly, and the unloading trajectory was approximately linear. Both the residual deformation and the hysteretic loop area became minimal. At the early stage of the test, the hysteretic loop areas increased continuously when the horizontal displacement and number of cycles increased. The specimen was destroyed rapidly with a poor ductility.

The hysteretic behavior of the CFRP-strengthened specimen SRC-2, which had no seismic-damage, was better than that of specimen SRC-3, which had moderate seismic damage, and specimen SRC-4, which had severe seismic damage. In addition, the hysteretic behavior of the CFRP-strengthened specimen SRC-3, which had moderate seismic damage, was better than that of the CFRP-strengthened specimen SRC-4,

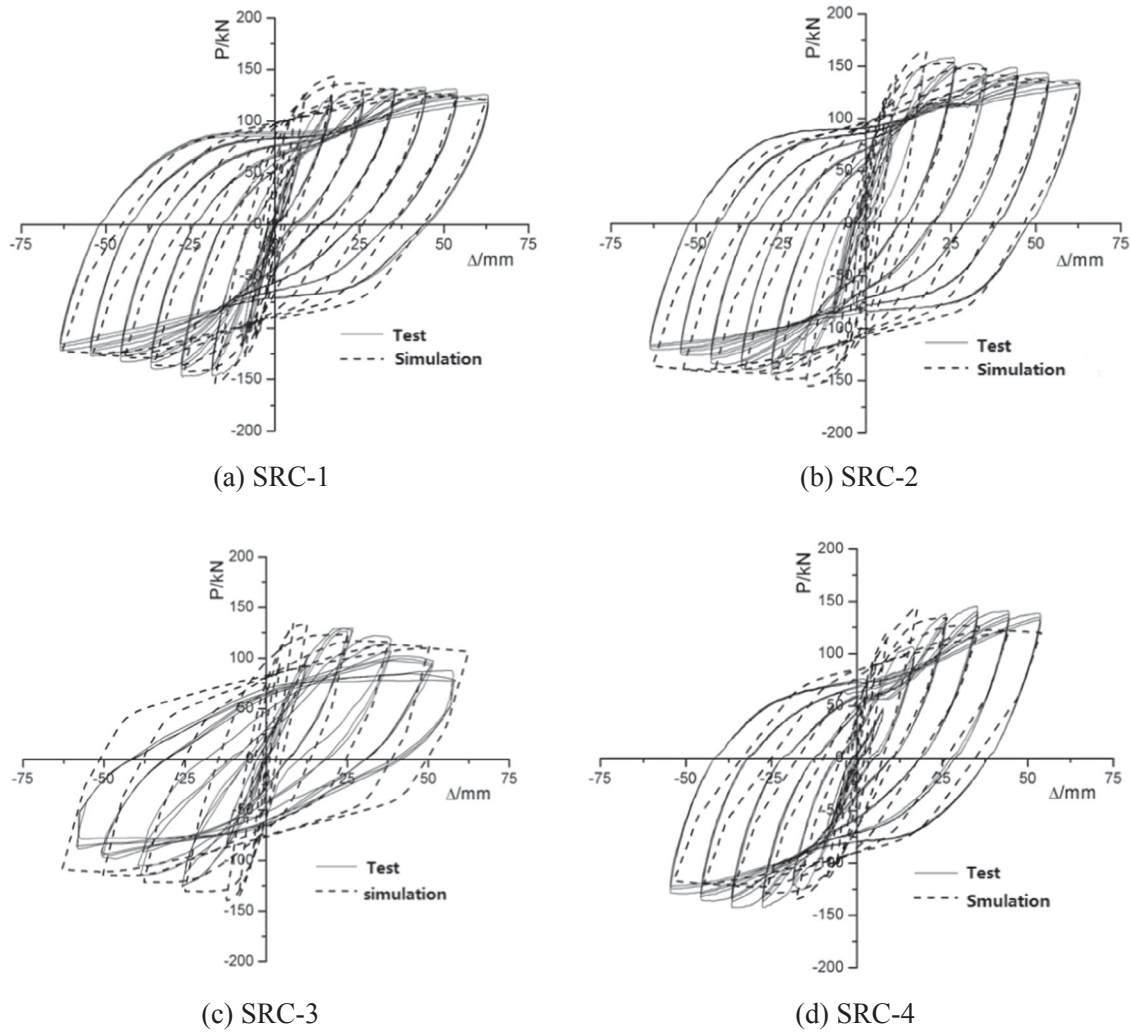


Fig. 4. Hysteretic loops of specimens.

which had severe seismic damage. The hysteretic loop of specimens SRC-2 and SRC-3 had good stability when the horizontal displacement increased to about 63 mm. However, specimen SRC-4 failed when the horizontal displacement reached to 54 mm. The presence of cross tie had a slight effect on the shape of the hysteretic curve of columns with T-shaped steel. There was slip between the CFRP and concrete influenced by the structural stability, and the bond between pre-damage concrete and steel was not so strong and could easily lead to slip. In the end, the draw shrinkage of the hysteretic curve shape appeared in the CFRP-strengthened columns. The cross tie enhances the ultimate bearing capacity by confining the concrete and preventing buckling of the longitudinal bar.

Comparison of the hysteretic curves of specimens SRC-1 and SRC-2 without any seismic damage reveals that the deformation and ductility of specimen SRC-2 are better than those of the prototype contrast specimen SRC-1. The manifestation of the seismic behavior of concrete of specimen SRC-2 was better due to its hysteretic curve roundness, deformability, energy dissipation capacity and longer loading cycles time.

3.3. Skeleton curve

The skeleton curves of all specimens are shown in Fig. 6. The results of the test of the characterization skeleton curves are shown in Table 3.

The skeleton curve reflects the characteristic of stress and deformation at different stages of the test of the specimen, which is an

important parameter to determine the feature points in the restoring force model. The cracking load defines the characteristics of the concrete cracks in the specimens, and the corresponding concrete cracks are defined as cracking displacements.

The general yielding moment method, which made a tangent of the skeleton curve through the origin O , intersecting at A with the horizontal line through the peak load, is depicted in Fig. 5. This method also made a vertical line through A , intersecting with the skeleton curve

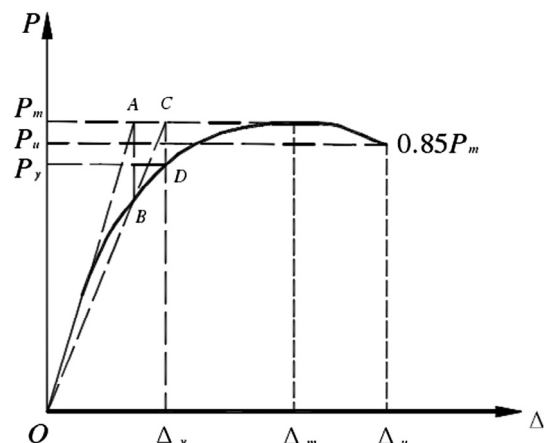


Fig. 5. Definition of yield point and failure point.

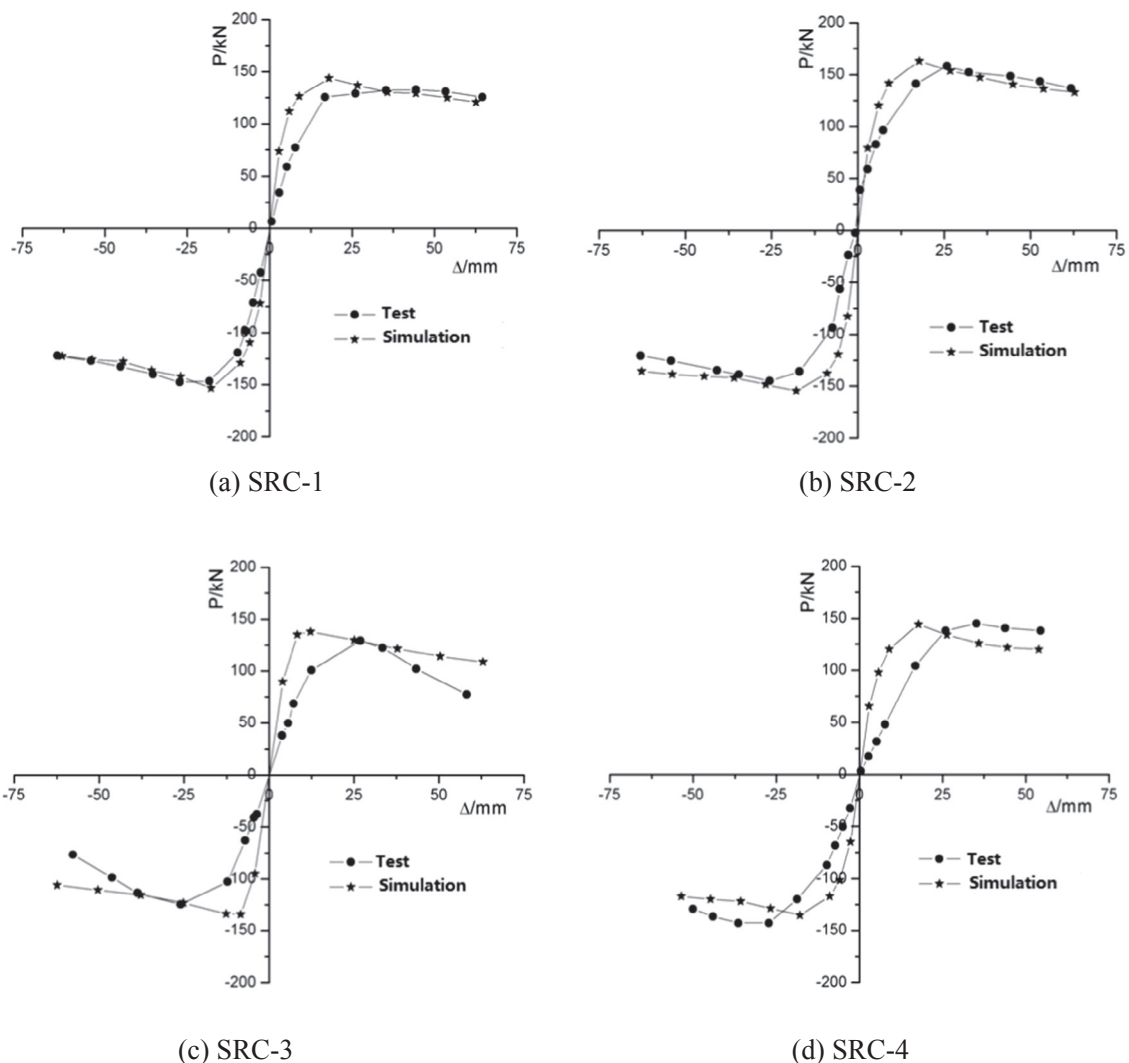


Fig. 6. Skeleton curves of specimens.

at *B*. When points *A* and *B* were connected and prolonged, point *C* appeared. The horizontal line and skeleton curve intersected at *D*, which is the yield point.

Ductility factors and lateral loads are two of the most common parameters used for the seismic evaluation of structural components. In the analysis of the skeleton curve, the positive loading direction was defined as when the wider flange of the inner structural steel was subjected to tension, while negative loading direction was defined as when it was subjected to compression.

In Fig. 6(a)–(d), the envelopes of the lateral load-displacement responses of all the tested specimens are compared to assess the effects of

the different strengthening situations and the degree of seismic damage on the ductility factors and lateral loads of the specimens. The experimental results for all columns are summarized in Table 3.

P_y and Δ_y are the yielding load and corresponding displacement, respectively. P_m is the maximum applied lateral load and Δ_m is the corresponding displacement. P_u is the failure load, which is defined as 85% of the maximum lateral load. P_m and Δ_u are the corresponding failure points, which are displaced. μ is the displacement ductility factor, calculated as Δ_u/Δ_y .

The skeleton curves shown in Fig.6 clearly show that the strengthening section appeared after the yielding, and the descending stage of

Table 3
Characteristic points of skeleton curves.

Specimen	Load direction	P_y /kN	Δ_y /mm	P_m /kN	Δ_m /mm	P_u /kN	Δ_u /mm	$\mu = \Delta_u/\Delta_y$
SRC-1	Positive	74.89	16.45	129.50	26.80	110.10	47.67	2.89
	Negative	94.55	17.28	124.64	25.93	143.79	49.18	2.85
SRC-2	Positive	75.63	17.19	162.16	36.52	142.44	58.35	3.40
	Negative	95.24	18.21	148.36	35.44	134.62	61.12	3.36
SRC-3	Positive	76.35	17.33	147.55	34.41	116.92	57.36	3.31
	Negative	98.38	18.32	145.66	33.25	122.94	58.87	3.21
SRC-4	Positive	86.12	16.78	145.10	30.12	125.21	54.29	3.24
	Negative	82.06	17.32	143.79	29.83	106.44	52.48	3.03

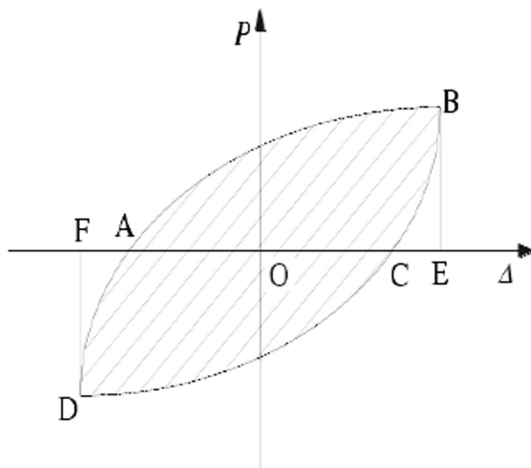


Fig. 7. Equivalent viscous damping coefficient h_e .

the CFRP-strengthened specimens appeared with gentle stability, which shows that the deformability of the specimens is good. With the change of the level of the earthquake damage, the strengthening of the specimens was only slightly influenced, while their ductility was clearly influenced.

The experimental results of all specimens are summarized in Table 3, and the following conclusions were drawn.

The ultimate deformability of the specimens strengthened with CFRP becomes better.

The ductility coefficient of specimens SRC-1 and SRC-2, with the same level of earthquake damage, increases in specimen SRC-2 from 2.89 to 3.40, an increase of about 17.65%, when the specimen SRC-2 is strengthened by CFRP.

The ductility coefficient decreases with the increase of the degree of damage. With the same degree of CFRP strengthening, the ductility coefficient of specimen SRC-2 is 3.40, and decreases to 3.31 in specimen SRC-3, and 3.24 in specimen SRC-4, which are decreases of about 2.65% in SRC-2 and 4.71% in SRC-4, where the earthquake damage level of the specimen changes from undamaged to moderate damage and to severe damage, respectively.

The ductility coefficient of specimen SRC-1 is less than that of specimens SRC-3 and SRC-4, which indicates that the strengthening with CFRP can effectively increase the ductility of the specimens. This indicates that the strengthening with CFRP can enhance the bearing capacity and ultimate displacement of the specimen. It mainly reflects the improvement of the mechanical behavior of the concrete, the deformation failure of the concrete on the tensile side at the bottom end of the column constrained by CFRP, and the delay of the yielding of the longitudinal reinforcement, which improves the ultimate bearing capacity of the specimen.

The maximum bearing capacity of specimens SRC-1 is 129.50 and it increases to 162.16 in SRC-2, 147.55 in SRC-3 and 145.50 in SRC-4, with rate of increase of about 36.27, 28.40 and 12.39% for SRC-2, SRC-3 and SRC-4, respectively. Meanwhile, the maximum displacement of the specimens is about 36.27, 28.40 and 12.39%, respectively, which improves the seismic behavior of the specimen.

The bearing capacity and displacement of the seismic-damaged CFRP-strengthened specimen can recover and even become better than the original specimen.

The characteristics of CFRP determine the strengthening and recovery capacity of the specimen, as well as whether the increase of the displacement of the specimen is better than its bearing capacity.

3.4. Energy dissipation capacity

The energy dissipation capacity, shown in Table 3, is defined as the

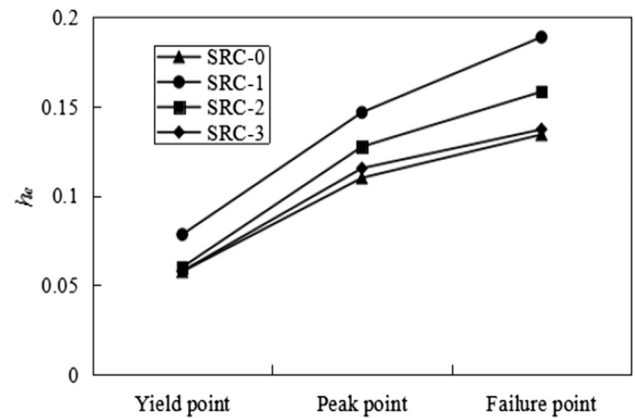


Fig. 8. Equivalent damping ratio.

dissipation capability of seismic energy in an earthquake, which is an important parameter to assess the seismic behavior of a structure.

During an earthquake, good energy dissipation capacity is conducive to the safety and stability of structural components, avoiding significant damage on structures [23].

The analysis of the energy dissipation capacity uses equivalent viscous damping coefficient as in the following equation.

$$h_e = \frac{A}{2\pi(S_{\Delta OBE} + S_{\Delta ODF})} \quad (1)$$

where A represents the area of a hysteretic loop, shown as the shadow area in Fig. 8; $(S_{\Delta OBE} + S_{\Delta ODF})$ is the area of a triangle corresponding to the maximum lateral load and the maximum horizontal displacement point of the hysteresis loop on the upper and lower sides. The hysteretic loop area, surrounded with dashed lines, and the horizontal axis are shown in Fig. 7.

The curves of the relationship between the equivalent viscous damping coefficient and the displacement of the specimens with different displacement levels under the first cyclic loading are shown in Fig. 8.

The curves depicted in Fig. 8 reveal that there is a certain impact on the energy dissipation capacity of the specimens strengthened with CFRP. The equivalent damping ratio of specimen SRC-1 is less than the equivalent damping ratio of specimens SRC-2, SRC-3 and SRC-4. Specimen SRC-2 has the maximal equivalent damping ratio of all the specimens.

With the increase of the displacement, the equivalent damping coefficient of all the specimens exhibits an upward trend. Clearly, the CFRP-strengthening has a great effect on the increase of equivalent damping coefficient.

3.5. Stiffness degradation

The stiffness degradation is defined as the decrease of the stiffness of the structure in an earthquake, which is an important parameter to assess the seismic behavior of a structure.

Based on the experimental results the mean value of the secant stiffness for the i th cycle was evaluated using the following ratio:

$$K_i = \frac{|P_{m,i}^+| + |P_{m,i}^-|}{|\Delta_{m,i}^+| + |\Delta_{m,i}^-|} \quad (2)$$

where K_i is the secant stiffness, which shows that the stiffness of each cycle can then be normalized with respect to the stiffness of the first cycle. In theory, the elastic stage never undergoes stiffness degradation.

The relationships between the K_i ratio and the imposed displacement are plotted in Fig. 9, which shows that as the horizontal displacement increases, the secant stiffness of the specimen gradually decreases. The specimens underwent stiffness degradation at the early

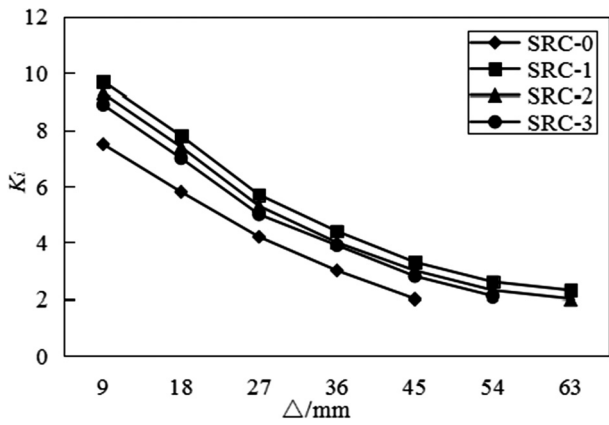


Fig. 9. Stiffness degradation curves of specimens.

stage of loading. The slope of the degradation curve is initially steeper, and then gradually tends to be moderate.

Stiffness degradation is more evident in the specimens strengthened with CFRP. Such a result indicated that increasing the level of the earthquake damage can improve the bearing capacity of the specimens within a certain range, but that will aggravate the stiffness degradation at the failure stage of loading.

The stiffness degradation of the specimens strengthened with CFRP is smaller than that of the original specimen, which indicated that CFRP can effectively repair the damaged specimens and improve its seismic resistant capacity.

3.6. Ductility coefficient

Ductility is a macro behavior of the structure, which is mainly used to characterize the deformation capacity of the specimens. The concrete of the compression side is not crushed due to the small bending moment, which causes the slightly inclined cracks on the side of the external concrete to rapidly develop upward along the steel flange. Ultimately, the failure of the bond with poor ductility occurred.

The ductility coefficient, shown in Table 3, is defined as ratio of the failure displacement to yielding displacement of the column.

$$\mu = \frac{\Delta_u}{\Delta_y} \tag{3}$$

With the same level of seismic damage, the ductility coefficient of the CFRP-strengthened specimen increases. The results indicated that the composite steel-concrete columns strengthened with CFRP can be used to delay ductility in the earthquake area. A comparison of the SRC-1 specimen with the CFRP-strengthened SRC-2 specimen revealed that the ductility of the latter is better.

With the same number of CFRP layers, the seismic damage is more severe and the ductility coefficient of the pre-damage specimen is smaller. Different levels of seismic damage lead to different ductility coefficient of specimens SRC-2, SRC-3 and SRC-4. The influence of the level of seismic damage on the ductility of the specimen cannot be ignored. The ductility of the pre-damaged specimens which are strengthened with CFRP decreases with the increase of the level of seismic damage.

Comparison of specimen SRC-1 with specimen SCR-4 indicate that the ductility of the severely-damaged specimen strengthened with CFRP is better. The ductility of the severely-damaged specimen strengthened

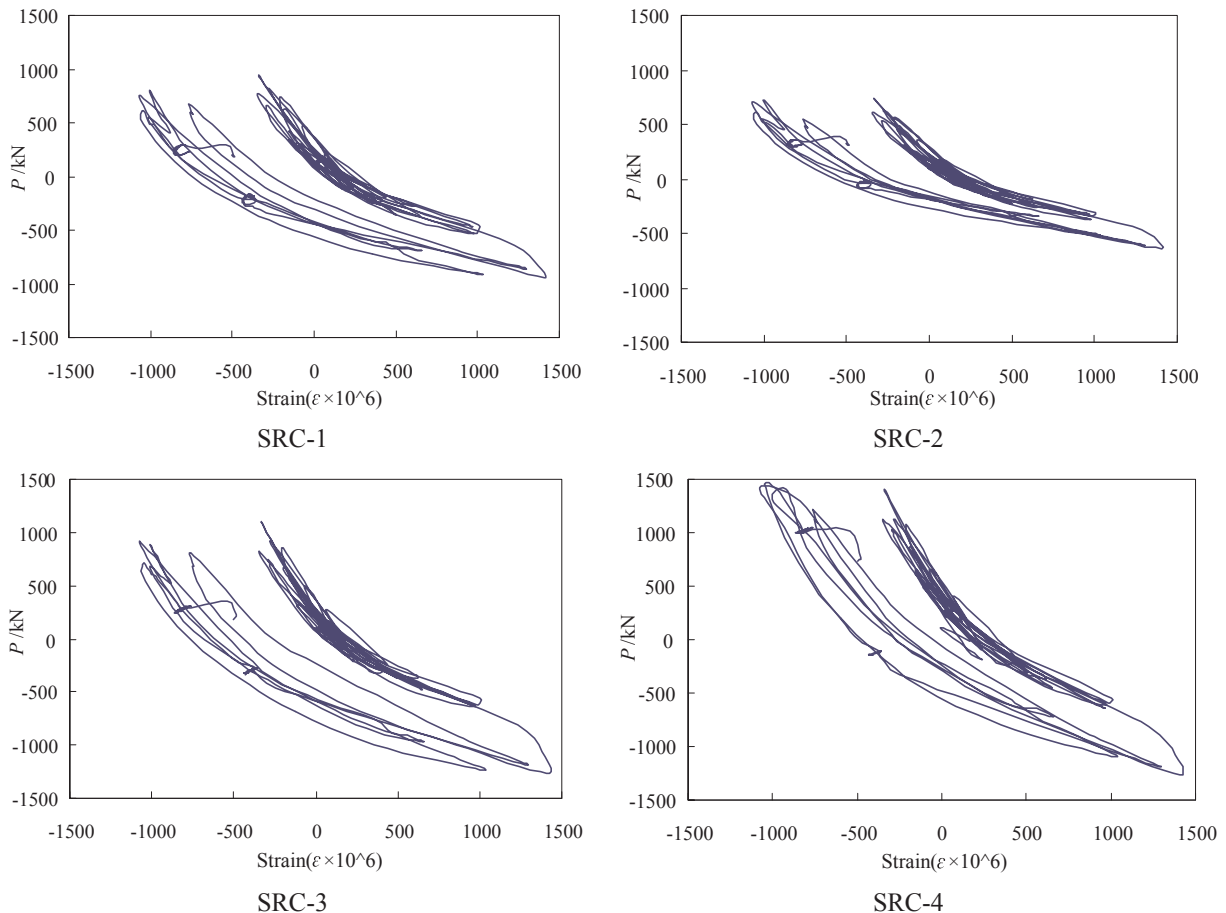


Fig. 10. Strains of section steel in the column of the bottom story.

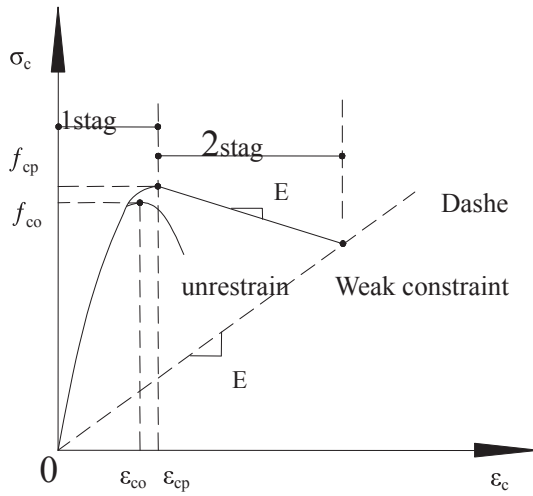


Fig. 11. Stress-strain relationship of concrete.

with CFRP increases significantly, and its ductility is better than that of the original specimen.

3.7. Strain analysis

The strains of the sections of steel in the composite steel-concrete frame columns at the bottom floor are shown in Fig. 10. The hysteretic characteristics of the load-strain curve of the sections of steel are obvious. The average strain is less than 1500×10^6 , and the residual strain is smaller after unloading. The change of the strains of specimen SRC-2 to SRC-4 with the increase of the level of damage is remarkable. Compared with specimen SRC-1, the strain of the strengthened specimen SRC-3 is larger, which shows that the deformation of the section of steel is a limited effect by the CFRP.

4. Finite element analysis

An analytical model is proposed for predicting the non-linear envelope response of the strengthened columns. The model is based on realistic material constitutive laws and accounts for the confinement effect of the added CFRP on the strength of the column.

4.1. Material modeling

For further research on the seismic performance of the post-earthquake composite steel-concrete frame, the column structure is strengthened with CFRP. The nonlinear finite element software ABAQUS was used to analyze the different tested specimens [33]. The stiffness recovery index, ω_c , which is defined as the stiffness recovery of concrete, is controlled under the cyclic loading [30].

When the load changed from tension to compression, as long as the crack was closed, the compressive stiffness would be recovered ($\omega_c = 1$); when the load changed from compression to tension, as long as the crack appeared, the tensile stiffness could be recovered ($\omega_c = 0$) when the crack appeared [30].

The constitutive relation of concrete without reinforcement is the following GB/T 50010-2010 “code for design of concrete structures”. There are several published studies on the FRP-confined concrete model and the mechanical properties of this material have been studied extensively. For further simulation and description the performance of the FRP-confined post-earthquake composite steel-concrete frame, the stress-strain model of the concrete confined with CFRP is proposed based on the stress-strain model described by Yang et al. [31], given by:

$$\sigma = f_{cp} \left[2 \left(\frac{\varepsilon_c}{\varepsilon_{cp}} \right) - \left(\frac{\varepsilon_c}{\varepsilon_{cp}} \right)^2 \right] \quad 0 \leq \varepsilon_c \leq \varepsilon_{cp} \quad (4)$$

$$\sigma = f_{cp} + E_2(\varepsilon_c - \varepsilon_{cp}) \quad \varepsilon_{cp} \leq \varepsilon_c \leq \varepsilon_{cc} \quad (5)$$

$$\varepsilon_{cc} = \frac{f_{cp} - E_2 \varepsilon_{cp}}{E_3 - E_2} \quad (6)$$

where f_{cp} and ε_{cp} are the defined peak stress and peak strain of the concrete after CFRP constraint, respectively; E_2 and E_3 are the defined tangent stiffness and tangent stiffness of concrete of the dropping straight line [29]. The formulas are as follows:

$$f_{cp} = \left[1 + 0.02 \rho_f \left(\frac{E_f}{(f'_{c0})^{3/2}} \right) \right] \cdot f_{c0} \quad (7)$$

$$\varepsilon_{cp} = \left[1 + 0.016 \rho_f \left(\frac{E_f}{f'_{c0}} \right) \right] \cdot \varepsilon_{c0} \quad (8)$$

$$E_2 = -44(1 - 2k_s) \frac{(f'_{c0})^3}{\rho_f E_f} \quad (9)$$

$$E_3 = 0.85 f_{c0} \quad (10)$$

where f_{c0} is the unconfined compressive strength of concrete in the rectangular section; f'_{c0} is the compressive strength of concrete of the standard cylinder; ε_{c0} is the peak strain of the confined concrete. Also, based on this study, $\varepsilon_{c0} = 0.002$. ρ_f , k_s are volume fraction and cross section shape coefficient of CFRP; E_f is the elastic modulus of CFRP; $\rho_f = 2t(b + h)/bh$; $k_s = rb + h/bh$; t is the total thickness of CFRP; r is the chamfer radius.

The longitudinal steel bar and section steel are analyzed by the classical ideal elastic-plastic model. CFRP is composed of orthogonal anisotropic materials, whose tensile stress along the fiber direction should be considered in the analysis, and the ideal elastic material is defined before it reaches the tensile strength. The stress-strain relationship of concrete is shown in Fig. 11 and the stress-strain relationship of the section of steel and CFRP is shown in Fig. 12.

4.2. Element type

The section of steel and concrete are reduced integration using eight-node solid elements (C3D8R), longitudinal bar and stirrups are dual-node truss element (T3D2), and CFRP is a four-node reduction integral membrane unit (M3D4R) [33]. Interaction on the contact surface between the section of steel and concrete are mainly normal and tangential whose spring elements were set as Spring 2. Spring stiffness in the normal direction is infinite, and that in the tangential should be set according to the bond strength. The finite element model is shown in Fig. 13.

Boundary conditions of the model and that of the testing are consistent, and the column bottom restrains the freedom of translational motion and the rotational motion on the direction of X, Y, Z to simulate the base binding effect of capitals placed on the rigid plate. Plate and capitals use bind (tie) connection.

The concentrated load was applied to simulate the vertical load that is applied to the jack while repeatedly applying horizontal displacement control at the loading point.

4.3. Comparisons of analytical and test results

The analytically predicted backbone envelope load-displacement responses against the measured cyclic response of the columns are shown in Figs. 4 and 6, which indicate that the non-linear analysis model predicts the envelope load-displacement response well.

The comparison of the testing and simulation of the ultimate

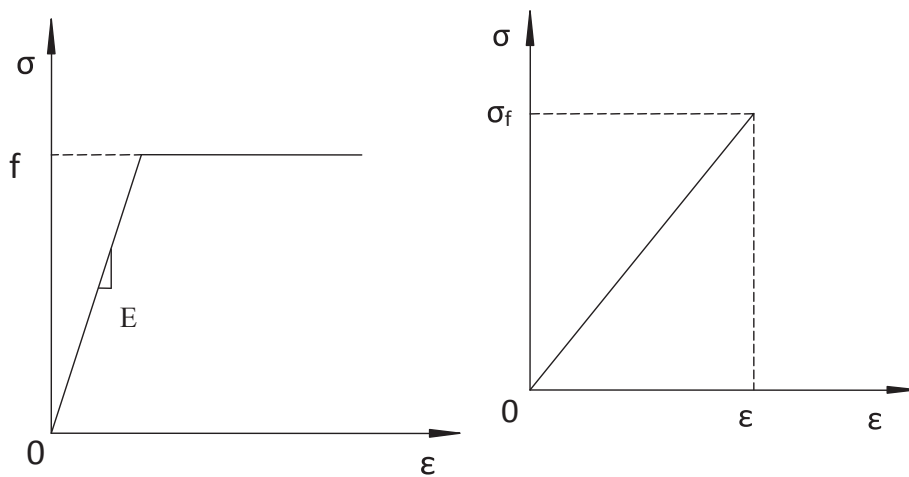


Fig. 12. Stress-strain relationship of steel and CFRP.

bearing capacity of the composite steel-concrete columns is summarized in table 4. The comparison indicated that the relative deviation between the tests and simulation is less than $\pm 10\%$. The mean is 5.23% and the variance is 0.014. The results of the model are consistent with those of the test.

5. Summary and conclusions

The effectiveness of seismic-damaged composite steel-concrete columns strengthened with CFRP to improve the seismic performance of composite steel-concrete columns was examined in this study. Based on the research results, the following conclusions can be drawn:

- (1) Strengthening the seismic-damaged composite steel-concrete column with CFRP sheets can improve its ductility. The level of seismic damage has a considerable influence on the behavior of the strengthened columns, the strengthening effects of the specimen with larger level of seismic damage on the ductility is better than those with lower level of seismic damage. The bearing capacity and displacement of the severe seismic damaged specimen strengthened with CFRP can be recovered and even be better than the original specimen.
- (2) Stiffness degradation of the specimens strengthened with CFRP decreases less than the original specimen, indicating that CFRP can effectively repair the damaged specimens and improve the seismic capacity. Both the bearing capacity and deformation capacity of the severe seismic damaged specimen strengthened with CFRP are slightly better than those of the original specimen. The ultimate bearing capacity of post-earthquake steel reinforced concrete frame

Table 4

Comparison of testing and simulation ultimate bearing capacities of composite steel-concrete columns.

Specimen	Test ultimate bearing capacity/kN	Simulation ultimate bearing capacity/kN	Relative deviation (%)
SRC-1	127.07	136.03	7.05
SRC-2	151.60	158.81	4.76
SRC-3	140.11	148.36	5.89
SRC-4	144.45	139.80	-3.22

- column structure was improved because it had a good working performance after strengthening with the carbon fiber sheet.
- (3) After moderate damage, the column with the recovered strengthening had, compared with the undamaged column, 10.41% of the average increase of the ultimate bearing capacity, 35.40% of the increase of the ultimate displacement and 14.53% of the increase of the ductility factor. And, regarding the column with the recovered strengthening after severe damage, its ultimate bearing capacity increased on average by 13.71%, the ultimate displacement increased on average by 32.68% and the ductility factor increased on average by 12.11%.
- (4) Strengthening have great influence on the specimens. Compared with the specimens without any reinforcement, specimens strengthened with carbon fiber sheets exhibit better hysteresis curve, skeleton curve, deformation and energy dissipation capacity, and smaller bearing capacity decline and stiffness degradation level. Accordingly, carbon fiber sheet should be applied in strict engineering to repair the damaged specimens and improve their

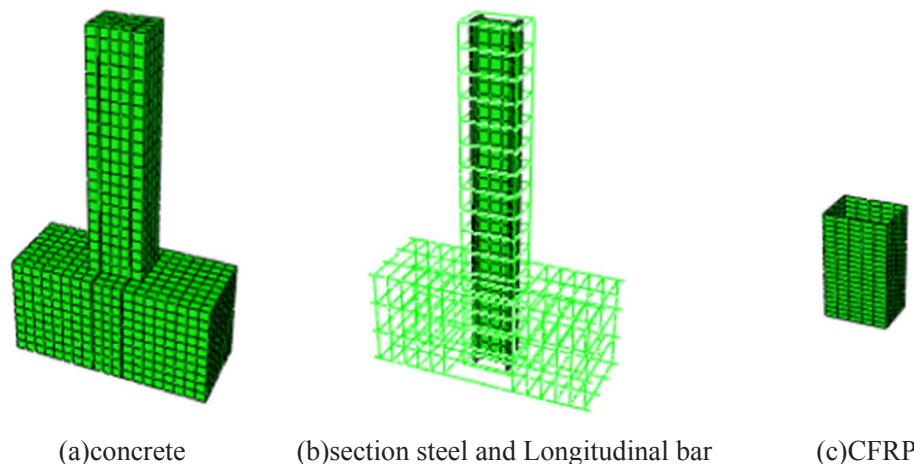


Fig. 13. Finite element model.

seismic performance.

- (5) The comparisons were made using the nonlinear finite element software, ABAQUS, to simulate four different conditions including the original column, undamaged strengthened column, moderate and severe damage. Based on the testing data, the hysteresis curves, skeleton curves, strength degradation and stiffness degradation of the post-earthquake seismic-damaged steel reinforced concrete frame column structures strengthened with CFRP were analyzed. A non-linear analysis model was developed for predicting the envelope load-displacement response, and the results of the model are consistent with those of the test.

6. Foundation item

This research is funded by ‘National Natural Science Foundation of China (CN)’ – ‘China’ (Grant No. 51108041, 51478048), ‘Young and Middle-aged Scientific and Technological Innovation Team Foundation of Hubei Province of China (CN)’ – ‘China’ (Grant No. T201303) and their support is gratefully acknowledged.

Appendix A. Supplementary material

Supplementary data associated with this article can be found, in the online version, at <http://dx.doi.org/10.1016/j.engstruct.2017.10.065>.

References

- [1] Nie JG, Tao MX, Huang Y, Chen G. Research advances of steel-concrete composite structural systems. *J Build Struct* 2010;31:71–80. [in Chinese].
- [2] Li J, Feng DC, Gao XL, Zhang YS. Stochastic nonlinear behavior of reinforced concrete frames. I: Experimental investigation. *J Struct Eng* 2016;142:0733–9445.
- [3] Zhang PZ, Hou S, Ou PJ. A beam-column joint element for analysis of reinforced concrete frame structures. *Eng Struct* 2016;118:125–36.
- [4] Feng DC, Li J. Stochastic nonlinear behavior of reinforced concrete frames. II: numerical simulation. *J Struct Eng* 2016;142:04015163.
- [5] Chen CC, Chen CC, Hoang TT. Role of concrete confinement of wide-flange structural steel shape in steel reinforced concrete columns under cyclic loading. *Eng Struct* 2016;110:0141–296.
- [6] Xu CX, Zeng L, Zhou Q, Tu X, Wu Y. Cyclic performance of concrete-encased composite columns with T-shaped steel sections. *Int J Eng Sci* 2015;61:455–67.
- [7] Guo ZX, Lin H, Liu Y. Experimental study on seismic behavior of SRC columns with different stirrup configuration. *J Build Struct* 2010;31:110–5. [in Chinese].
- [8] Leon R. An experimental study on strength and serviceability of reinforced and steel fiber reinforced concrete (SFRC) continuous composite slabs. *Eng Struct* 2016;114:171–80.
- [9] Lampropoulos AP, Paschalis SA, Tsioulou OT, Dritsos SE. Strengthening of reinforced concrete beams using ultra high performance fibre reinforced concrete (UHPRC). *Eng Struct* 2016;106:370–84.
- [10] RUCT ENT, Noshiravani, E. Brühwiler. Analytical model for predicting response and flexure-shear resistance of composite beams combining reinforced ultrahigh performance fiber-reinforced concrete and reinforced concrete. *J STG* 2014; 140: 1299–28.
- [11] Yoo DY, Banthia N, Yoon YS. Flexural behavior of ultra-high-performance fiber-reinforced concrete beams reinforced with GFRP and steel rebars. *Eng Struct* 2016;111:246–62.
- [12] Wang X, Sayed AM, Wu ZS. Modeling of the flexural fatigue capacity of RC beams strengthened with FRP sheets based on finite-element simulation. *J Struct Eng* 2015;141:04014189.
- [13] Yin SF, Hu KX. Numerical simulation for the pseudo-static test of strengthened RC columns with earthquake-damage based on opensees. *Eng Struct* 2015;31:145–51.
- [14] ACI Committee 318. Building code requirements for structural concrete (ACI 318-05) and commentary (ACI 318R-05). American Concrete Institute; 2005 [in American].
- [15] YB 9082-2006. Technical specification of steel-reinforced concrete structures. National Development and Reform Commission of the PRC; 2006 [in Chinese].
- [16] JGJ 138-2001. Technical specification for steel reinforced concrete composite structures. Architecture Industrial Press of China; 2001 [in Chinese].
- [17] AIJ-SRC. Standard for the calculation of steel-reinforced concrete structures. Architectural institute of Japan; 2010 [in Japanese].
- [18] Kim SH, Choi JH. Repair of earthquake damaged RC columns with stainless steel wire mesh composite. *Adv Struct Eng* 2010;13:393–402.
- [19] Zhao G, Cao FB. Seismic behavior of reinforced concrete crack-short columns strengthened with CFRP. *Earthq Resistant Eng Retrofitting* 2010;132:15–9. [in Chinese].
- [20] Xu CX, Peng W, Xu KL, Zhou L. Experimental research on seismic behavior of CFRP-strengthened seismic-damaged exterior joints in composite frame consisting of CFSST columns and steel beams. *J Struct Eng* 2014;135:69–76.
- [21] Zhang YB. Experimental study on seismic behavior of RC frame columns strengthened with new material. Tongji University, Shanghai; 2012 [in Chinese].
- [22] Wang ZM. Experimental study and theoretical analysis on the vibration table of seismic damage RC frame strengthened with new material. Tongji University, Shanghai; 2012 [in Chinese].
- [23] Karayannis CG, Sirkelis G. Strengthening and rehabilitation of RC beam-column joints using carbon-FRP jacketing and epoxy resin injection. *J Earthq Eng Struct D* 2008;37:769–90.
- [24] Ozbakkaloglu T, Saatcioglu M. Seismic performance of square high-strength concrete columns in FRP stay-in-place formwork. *J Struct Eng, ASCE* 2007;133:44–56.
- [25] Ozbakkaloglu T, Saatcioglu M. Seismic behavior of high-strength concrete columns confined by fiber reinforced polymer tubes. *J Compos Constr* 2006;10:538–49.
- [26] Idris Y, Ozbakkaloglu T. Behavior of square fiber reinforced polymer-high-strength concrete-steel double-skin tubular columns under combined axial compression and reversed-cyclic lateral loading. *Eng Struct* 2016;118:307–19.
- [27] Idris Y, Ozbakkaloglu T. Seismic behavior of high-strength concrete-filled FRP tube columns. *J Compos Constr* 2013;17:04013013.
- [28] Idris Y, Ozbakkaloglu T. Seismic behavior of FRP-high-strength concrete-steel double skin tubular columns. *J Struct Eng, ASCE* 2012;140:1299–328.
- [29] Professional Standard of the People's Republic of China. Specifying of Testing Methods for Earthquake Resistant Building (JGJ 101–96). Beijing, China: China Architecture and Building Press; 1997. [in Chinese].
- [30] Hou PJ. Research on the seismic damage mode of steel reinforced high strength and high performance concrete frame. Xi' An: Xi'an University of Architecture and Technology; 2009 [in Chinese].
- [31] Yang W, Wu G, Wu ZS, Gu DS, Guo ZS. Ductility analysis of FRP-confined short rectangular reinforced concrete columns. *J Earthquake Eng Eng Vibrat* 2009;29:71–6. [in Chinese].
- [32] Ozbakkaloglu T, Jian CL. Axial compressive behavior of FRP-confined concrete: experimental test database and a new design-oriented model. *Compos Part B-Eng* 2013;55:607–34.
- [33] Jian CL, Ozbakkaloglu T. Confinement model for FRP-confined high-strength concrete. *J Compos Constr, ASCE* 2013;18:2537–47.